Materials Science and Engineering A 528 (2011) 3398–3403

Contents lists available at ScienceDirect

Materials Science and Engineering A

journal homepage: www.elsevier.com/locate/msea

Strain hardening and softening in a nanocrystalline Ni–Fe alloy induced by severe plastic deformation

S. Ni[a], Y.B. Wang[a], X.Z. Liao[a,*], S.N. Alhajeri[b], H.Q. Li[c], Y.H. Zhao[d], E.J. Lavernia[d], S.P. Ringer[e], T.G. Langdon[f,g], Y.T. Zhu[h]

[a] School of Aerospace, Mechanical and Mechatronic Engineering, The University of Sydney, Sydney, NSW 2006, Australia
[b] Department of Manufacturing Engineering, College of Technological Studies, PAAET, Shuwaikh 70654, Kuwait
[c] Los Alamos National Laboratory, Los Alamos, NM 87545, USA
[d] Department of Chemical Engineering and Materials Science, University of California, Davis, CA 95616, USA
[e] Australian Centre for Microscopy and Microanalysis, The University of Sydney, NSW 2006, Australia
[f] Department of Aerospace and Mechanical Engineering and Materials Science, University of Southern California, Los Angeles, CA 90089-1453, USA
[g] Materials Research Group, School of Engineering Sciences, University of Southampton, Southampton SO17 1BJ, UK
[h] Department of Materials Science and Engineering, North Carolina State University, Raleigh, NC 27659-7919,USA

ARTICLE INFO

Article history:
Received 17 November 2010
Received in revised form 5 January 2011
Accepted 6 January 2011
Available online 12 January 2011

Keywords:
Severe plastic deformation
Nanocrystalline materials
Strain softening
Strain hardening
Dislocation density

ABSTRACT

The strain response of an electrochemically deposited nanocrystalline Ni–20 wt.% Fe alloy processed by high-pressure torsion (HPT) was investigated by monitoring changes in hardness. Strain hardening was observed in the very early stage of HPT, followed by strain softening before the onset of a second strain hardening stage. Structural investigations revealed that the two hardening stages were associated with an increase in dislocation density, whereas the strain softening stage was accompanied by a reduction in the dislocation and twin densities, thereby demonstrating the main dependence of hardness on the dislocation density in this material. Grain growth occurred during HPT and its role in the hardness evolution is also discussed.

1. Introduction

There has been considerable interest over the last decade in producing bulk ultrafine-grained (UFG, <1 μm) and nanocrystalline (nc, <100 nm) materials for superior mechanical properties via severe plastic deformation (SPD) in which intense plastic straining is achieved under a high confined pressure [1]. The most developed SPD techniques include equal-channel angular pressing (ECAP) [2] and high-pressure torsion (HPT) [3]. Available experimental evidence suggests that HPT is more effective in producing smaller grains than ECAP [4–6].

Extensive studies have been carried out to understand SPD-induced grain refinement and the effect of the grain refinement and other SPD-induced microstructural evolution on the mechanical properties of materials [2,3,7]. At early stages of an SPD process, coarse grains transform into elongated fine grains with lamellar grain boundaries that gradually evolve from low angles to high angles [8,9]. Further plastic deformation results in a transition from the lamellar structure to an equiaxed UFG or nc structure [8,9]. The SPD process also introduces a significant increase in the dislocation density in materials. The combined effect of grain refinement and increased dislocation density leads to a significant strain hardening or work hardening [9–11]. Further plastic deformation reduces the total dislocation density by reducing the volume fraction of grain boundaries. This leads to slight strain softening and, at least to some extent, restores the strain hardening capability that increases the ductility of materials [9,12–14]. Strain softening during grain refinement has been widely reported and various mechanisms have been proposed, including the formation of shear bands promoted by the reorientation of grains [15], a reduction in the dislocation density via an annihilation of dislocations at grain boundaries [16] and dynamic recovery [9,17].

The general SPD-induced grain refinement described above reaches a threshold and there is a minimum average grain size that is achieved for any specific material and SPD process [18]. Both intrinsic material properties such as stacking fault energy and extrinsic processing parameters [18,19] are factors that determine this minimum average grain size. One of the factors leading to a minimum grain size is that SPD processes

* Corresponding author. Tel.: +61 2 9351 2348; fax: +61 2 9351 7060.
E-mail address: xiaozhou.liao@sydney.edu.au (X.Z. Liao).

0921-5093/$ – see front matter © 2011 Elsevier B.V. All rights reserved.
doi:10.1016/j.msea.2011.01.017

also result in grain growth. The minimum grain size is determined by a dynamic balance between the grain refinement process and the grain growth process. It is difficult to investigate SPD-induced grain growth phenomena using coarse-grained materials because the dominant evolution phenomenon is grain refinement. By contrast, SPD-induced grain growth has been readily observed under various plastic deformation processes in materials where the starting grain sizes were much smaller than the minimum grain sizes achieved by SPD-induced grain refinement [20–24].

Two SPD-induced grain growth mechanisms have been reported. For grains larger than ~100 nm, grain growth appears to occur predominantly via stress coupled grain-boundary migration in which a grain grows at the expense of other neighboring grains [25]. For grains much smaller than ~100 nm, grain growth appears to occur via grain rotation and coalescence [26–29]. A grain growth process is usually also accompanied by other structural evolution processes, including the evolution of twin and dislocation densities [29–33].

SPD-induced grain growth and other microstructural phenomena affect significantly the mechanical behaviour of materials. For example, deformation twinning in nc palladium during grain growth induced by HPT led to an increase in the microhardness from 280 to 394 [34]. A significant increase in dynamic plasticity accompanied by a high strength was realized in a nc Ni–Fe alloy under dynamic loading because of a deformation-induced detwinning process that may have played a primary role in relieving stress concentrations, leading to flow softening [35]. Li et al. [21,31] recently reported that slight plastic deformation via cold rolling of a nc Ni–Fe alloy resulted in a reduction of dislocation density and this produced strain softening.

A previous investigation focusing on the structural evolution of a nc Ni–20 wt.% Fe alloy processed by HPT to different strain values showed that the grain growth mechanism has a significant effect on the evolution of the dislocation density [32]. The evolution of dislocation density and other structural features will affect significantly the mechanical behaviour of the material. However, the relationship between the structural evolution and the mechanical properties in the material is not yet clear. In this study, we conducted detailed hardness testing to characterize the HPT-induced hardness evolution. Combining with the previous results on the grain size and dislocation density evolution deduced from X-ray diffraction (XRD) measurements and transmission electron microscopy (TEM) observations [32], as well as new TEM results on other structural features, we discuss how the overall structural evolution affects the hardness of the material.

2. Experimental procedures

We studied an electrochemically deposited nc Ni–20 wt.% Fe alloy with a homogeneous microstructure purchased from the Integran Technologies Inc. (Pittsburgh, USA). The alloy was synthesized using the method described in Ref. [36]. The as-deposited material was a non-equilibrium supersaturated solid solution with a single phase face-centred cubic structure [36]. Specimens for HPT processing were sectioned into disks with a diameter slightly less than 10 mm and a thickness of ~1.5 mm. These disks were polished on both sides using sand papers (400–2000 grade) until their thickness reached 0.8 mm. The HPT process was then conducted using a quasi-constrained HPT facility [3]. Disks were subjected to ¼-revolution HPT under an applied pressure of 3 GPa and 2-, 3-, 5-, and 10-revolution HPT under an applied pressure of 6 GPa, respectively, using a rotation rate of 1 rpm.

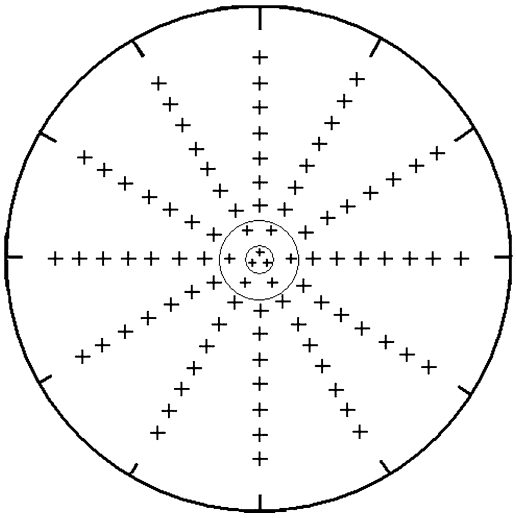

Fig. 1. Schematic illustration of the positions for taking the hardness measurements.

After HPT processing, the disks were mechanically polished to produce a mirror-like surface using diamond lapping films (30–1 μm) for hardness testing. Hardness measurements were taken using a Leco LV700AT hardness tester equipped with a Vickers indenter and with a load of 10 kg applied at each point for 15 s. The Vickers hardness Hv obtained in this way had units of kgf/mm^2 which may be converted to GPa using 1 kgf/mm^2 = 0.009807 GPa [37]. The hardness was measured at points with radius values of r = 1, 1.5, 2, 2.5, 3, 3.5 and 4 mm and these values were averaged from 12 datum points positioned by a rotational increment of 30° around the disk centre. The hardness values at the disk centre and at a radius value of 0.5 mm were averaged from 3 datum points by a rotational increment of 120° and from six data by a rotational increment of 60° around the disk centre, respectively. The points in a disk where hardness was tested are shown schematically in Fig. 1. The error bar for each mean hardness value was obtained from the tested highest hardness value to the lowest value.

The samples for TEM investigation were prepared by cutting small disks with a diameter of 3 mm at selected areas in the HPT disks. The TEM disks were prepared using standard techniques and TEM investigations were carried out using a JEOL JEM 3000F microscope operating at 300 kV.

3. Experimental results

3.1. Hardness evolution

Fig. 2 charts the Vickers hardness values at different radial positions on the as-deposited disk, the ¼-revolution HPT disk under a pressure of 3 GPa, and the 2-, 3-, 5-, and 10-revolution HPT disks under a pressure of 6 GPa. The Vickers hardness increased from 4.8 GPa in the as-deposited sample to 5.2 and 5.6 GPa at the centres of the disks subjected to pressures of 3 and 6 GPa, respectively. The Vickers hardness of the ¼-revolution HPT disk experienced a moderate increase from the disk centre to the edge, indicating that strain hardening occurred in the initial stages of plastic deformation. It is interesting to note that strain softening occurred at the edge of the 2-revolution HPT disk and the lowest hardness in the disk approached that of the as-deposited sample. Strain softening also occurred in part of the 3-revolution disk within radius values from 1.5 to 2.5 mm and the lowest hardness was around 5.1 GPa which is a little higher than the lowest hardness found in the 2-revolution disk. It should be noted that strain softening has been reported also in the early stages of cold rolling in a nc Ni–Fe alloy with a

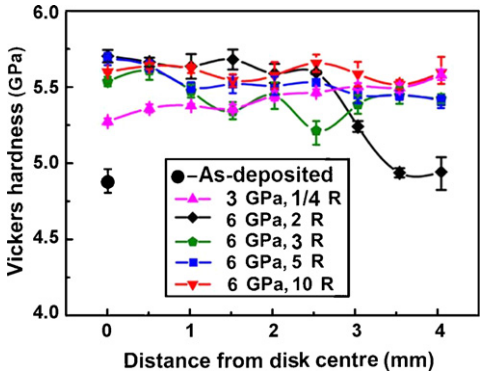

Fig. 2. Vickers hardness plotted against distance from the centre of disk samples after HPT processing under 3 GPa pressure for ¼ revolutions and under of 6 GPa pressure for 2, 3, 5, and 10 revolutions, respectively. The hardness of the as-received material is also presented.

composition similar to the alloy used in this investigation [21,31]. The hardness in the 5- and 10-revolution disks is reasonably uniform with some fluctuations between 5.4 and 5.6 GPa.

In order to better understand the effect of HPT-induced plastic deformation on the hardness evolution, the hardness values are plotted as a function of the von Mises equivalent strain in Fig. 3, where the equivalent strain, ε, is defined as $\varepsilon = 2\pi Nr/\sqrt{3}h$, where r is the distance from the disk centre, h is the thickness of the disk and N is the number of HPT revolutions [38]. Fig. 3(a) shows the relationship between the hardness and equivalent strain up to a value of $\varepsilon = 4.5$, recorded in the disk subjected to a ¼ revolution under 3 GPa, which indicates clearly that strain hardening occurred in the initial stages of HPT. For the convenience of further discussion, this equivalent strain regime is designated as deformation stage I. Fig. 3(b) shows the hardness–strain relationship for higher values of equivalent strain recorded from the disks subjected to 2-, 3-, 5-, and 10-revolution HPT under 6 GPa. Consistent with

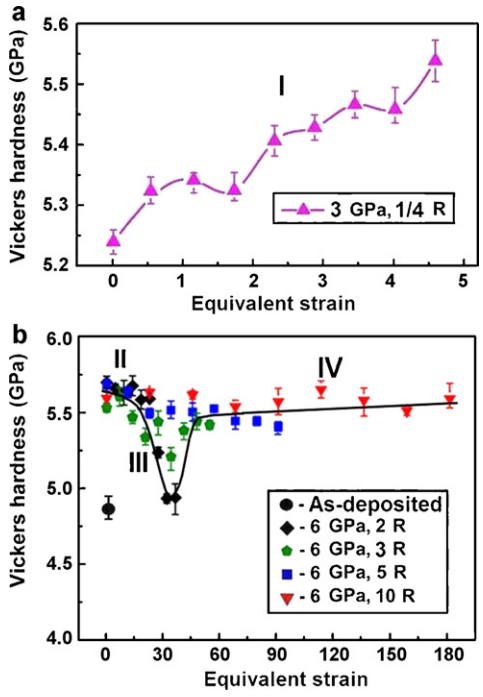

Fig. 3. (a) Vickers hardness plotted against the von Mises equivalent strain for the sample processed by HPT under 3 GPa pressure for ¼ revolutions; (b) Vickers hardness plotted against the equivalent strain for the samples processed by HPT under 6 GPa for 2, 3, 5, and 10 revolutions.

Table 1
Dislocation densities calculated by XRD data and average grain sizes measured from TEM images of disks at different deformation stages. The ranges of equivalent strain at different deformation stages are also listed.

Deformation stage	Equivalent strain	Dislocation density (m^{-2})	Average grain size (nm)
As-deposited	0	2.2×10^{15}	21
I	0–4.5	3.6×10^{15}	22
II	4.5–20	5.8×10^{15}	30
III	20–35	4.1×10^{15}	35
IV	35–182	6.0×10^{15}	50

the results in Fig. 3(a), the hardness also increases dramatically in the initial stages of HPT, reaching a maximum of 5.6 GPa where this is designated as deformation stage II. Strain softening starts to occur at an equivalent strain value of about 20 and the hardness decreases to a minimum of ~4.9 GPa at a strain value of about 35. The strain softening process is designated stage III of the deformation. Rapid strain hardening occurs again with further deformation and reaches a hardness plateau of ~5.6 GPa at an equivalent strain value of around 45. Beyond this point, further deformation gives no significant hardness change. The second strain hardening stage is designated as deformation stage IV, as indicated in Fig. 3.

Review of the published literature shows that a reasonable level of hardness and microstructural homogeneity is achieved in disks subjected to 5 or more HPT revolutions [39,40]. This is because the real shear strain in an HPT process is complex and it is not easily explained using the ideal shear strain model [41,42]. The hardness homogeneity in the 5- and 10-revolution disks in this investigation is consistent with these earlier reports. In addition, one datum point at an equivalent strain value of ~34 obtained from the disk subjected to 5-revolution HPT does not demonstrate strain softening and significantly deviates from that of the 2- and 3-revolution disks.

3.2. Evolution of grain size and dislocation density

For the convenience of the analysis of the relationship between structural evolution and hardness evolution, the average grain sizes estimated from TEM images and dislocation densities calculated from XRD data at different deformation stages [32] are summarized in Table 1. The TEM and XRD data were obtained from the ¼-revolution HPT disk for deformation stage I, the central part ($0 < d < 2.5$ mm) and edge part (2.5 mm $< d < 5$ mm) of 2-revolution HPT disk for deformation stages II and III, respectively, and the edge parts of 5- and 10-revolution HPT disks for deformation stage IV. A twinned grain was treated as a single grain when evaluating average grain sizes. Grain growth occurred continuously via grain rotation and coalescence throughout the HPT process such that the average grain size reached ~50 nm at deformation stage IV from ~21 nm of the as-deposited material. In contrast, the dislocation density does not evolve monotonously. Note that the minor average grain size difference between the as-received sample and the sample at deformation stage I may be within statistical error.

The average dislocation density of the as-deposited material was 2.2×10^{15} m^{-2} but it increased to 3.6×10^{15} m^{-2} in material having equivalent strain values between 0 and 4.5 in stage I of the deformation. In stage II the average XRD dislocation density reached 5.8×10^{15} m^{-2}, and in stage III, with a relatively narrow range of equivalent strain values of about 20–35, the average dislocation density dropped significantly to 4.1×10^{15} m^{-2}. The dislocation density at the place with an equivalent strain of about 35 may be similar to that of the as-deposited material because of the similarity of their hardness but this was not confirmed experimentally because of the difficulty of conducting XRD measurements on very small amounts of material. The dislocation density increased

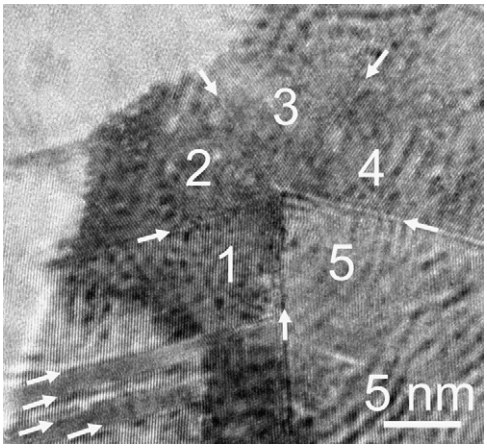

Fig. 4. A TEM image of a grain with high density of twins before de-twinning. A fivefold twin and some single twins are visible in the grain. The twin boundaries are indicated by white arrows and each twin domain of the fivefold twin is marked with 1–5, respectively.

again as deformation continued, reaching a plateau of around $6.0 \times 10^{15}\,m^{-2}$ in stage IV. Note that the errors in these dislocation density measurements are less than 6% which is significantly smaller than the dislocation density changes between different deformation stages [32].

3.3. De-twinning

Fig. 4 shows a typical TEM image of a high density of growth twins in a grain in the as-deposited material. A fivefold twin and some single twins exist in the grain. The twin boundaries are indicated by white arrows and each twin domain of the fivefold twin is marked with 1–5, respectively. High densities of growth twins are often observed in electrodeposited face-centred cubic materials [43,44]. Careful examination revealed that high densities of growth twins were retained throughout the deformation stage I. However, the extent of the twinning started to decrease at stage II and it was reduced significantly during stage III. Few twins were visible thereafter. The twin boundaries observed in the as-deposited material were usually atomically flat as is evident in Fig. 4. However, zigzag-shaped twin boundaries were found at stages II and III.

Fig. 5(a) shows a low magnification twin morphology observed at stage II and Fig. 5(b) shows a high-resolution TEM image of the area marked with a white rectangle in Fig. 5(a). As shown in Fig. 5(b), two twin boundary steps are visible and marked with white arrows. Several partial dislocations exist at each of the two steps (3 partials at the left step and 4 at the right step). The height of these steps is equal to the number of the accumulated partials multiplied by the $\{1\,1\,1\}$ inter-planar distance [45,46]. These partials could be generated from the grain boundaries that intersect with twin boundaries during plastic deformation. Partial dislocation formation from grain boundaries usually leads to a significant increase in twinning in nc materials [47–49]. It can also result in de-twinning if a partial forms and glides on the twin plane neighboring the matrix [50]. Deformation-induced de-twinning in electrodeposited Ni–Fe alloys has been reported [35] but the precise mechanism was not investigated experimentally. Recent in situ TEM and computational modeling investigations [51] suggest that nanotwins are unstable and that de-twinning can easily occur for thin twins. The driving force was mainly attributed to a variation in the excess energy of a coherent twin boundary. We believe that grain sizes also play a significant role in this de-twinning phenomenon. Further investigation is needed to understand the physics behind the de-twinning phenomenon.

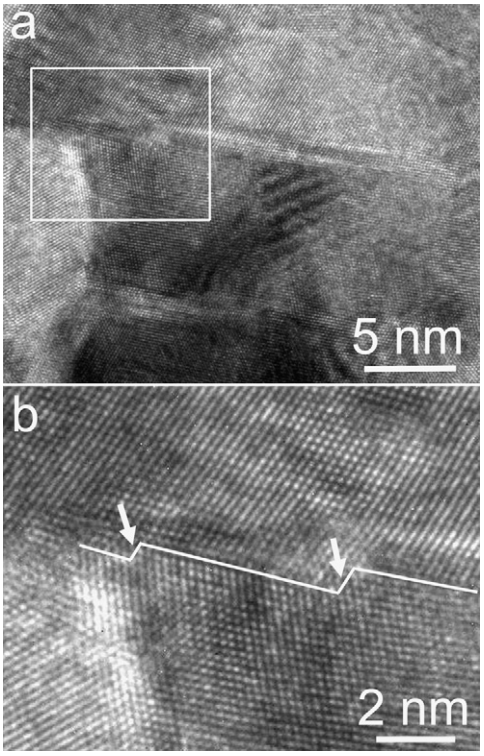

Fig. 5. (a) A TEM image of twin morphology observed in deformation stage II; (b) a high-resolution TEM image of the area marked with a white square in (a) with two steps along the twin boundary indicated with white arrows.

4. Discussion

This study reveals a unique HPT-induced hardness evolution in a nc Ni–Fe alloy: strain hardening occurs at the initial stages of deformation, followed by a strain softening and subsequent further strain hardening. The hardness evolution is a consequence of the microstructural evolution of the material. Comparing Table 1 and Fig. 3, we can see that the rapid hardening in stages I and II mainly results from the dislocation accumulation due probably to the high density of dislocation sources existing at the grain boundaries of the as-deposited sample, by which the rate of dislocation generation was relatively high at the initial stages of deformation. High densities of dislocations were pinned by solute atoms or interacted with pre-existing twin boundaries, leading to strain hardening, while the slight grain growth and de-twinning may consume some of the hardening in stage II. The softening in stage III by comparison with stage II could be attributed to the evident decrease in dislocation and twin densities. High densities of dislocations within nc grains were unstable, thus further deformation of the material forced the dislocations, which were initially weakly pinned by solute atoms, to glide towards, and disappear at, grain boundaries when an external force was available to activate dislocation slip [32]. Therefore, the rate of dislocation disappearance at grain boundaries due to dislocation slip surpassed that of dislocation generation, leading to a reduction in dislocation density [32]. Twins have been suggested as dislocation obstacles in small grains and dislocation motion may be hindered by twin boundaries which produce dislocation pile-ups along the boundaries [43,52]. Twins have been claimed as one of the main reasons for strain hardening [34] and de-twinning has been reported to lead to strain softening [35]. Therefore, the de-twinning phenomenon observed in this study should also play a role in hardness evolution. The minor grain growth from 30 nm (stage II) to 35 nm (stage III) may make a very small contribution to the softening. Further deformation (stage IV) re-accumulated dislocations in

the grain interiors, thereby increasing the dislocation density and leading to a further increase in hardness. It has been demonstrated that the formation of a large number of Lomer–Cottrell (L–C) locks, which is a direct consequence of the deformation-induced grain growth via grain rotation and coalescence [32], is responsible for the second increase in the dislocation density. During the grain rotation process, sub-grain boundary dislocations, which existed three-dimensionally, glided away from the sub-grain boundaries on different {1 1 1} planes. These dislocations might meet, interact and tangle with each other, forming L–C locks [32]. Both experimental evidence [53] and molecular dynamics simulations [54,55] show that an L–C lock structure is extended on two {1 1 1} planes, which provides a strong barrier to the motion of dislocations and plays a critical role in strain hardening. Moreover, the L–C barriers provide extra sources for dislocation generation, which can enhance the dislocation storage capability to achieve good ductility as well as strength in the materials.

There have been several reports on strain softening in nc materials and these have been rationalized on the basis of various mechanisms. Billard et al. [56] observed strain softening in aluminum nano-powder during hot isostatic pressing which could be explained by the mechanism of annihilation of dislocations at grain boundaries and dynamic recovery. Yang et al. [14] reported strain softening of nc nickel due to coarsening which was induced by grain boundary migration. Huang et al. [57] reported that annealed nanostructured aluminum was hard because of the lack of dislocations to facilitate plastic deformation and was softened by cold rolling which introduced a large number of dislocations that makes plastic deformation easy when the metal is stressed. The fundamental mechanism that rationalizes low plasticity on the basis of a low dislocation density was demonstrated by Shan et al. [58] using in situ TEM nanocompression experiments on submicrometer-sized Ni pillars. However, this mechanism is valid only when the dislocation density is low. In a nc metallic alloy like the Ni–Fe alloy studied here, the dislocation density is much higher than those reported in pure metals ($\sim 3.6 \times 10^{15}\,m^{-2}$ for the present Ni–Fe alloy compared with $\sim 5.3 \times 10^{13}\,m^{-2}$ for pure Al after annealing [57] and completely dislocation-free for pure Ni pillars after compression many times [58]), so that further increasing the dislocation density can only make dislocation motion more difficult because of the strong interaction among the dislocations. As a result, the strain softening mechanism observed in this material is different from that in nc pure Al or Ni. Note also that strain softening induced by a dislocation density reduction was reported in a nc Ni–18 wt.% Fe alloy during cold rolling [31].

5. Conclusions

A comprehensive investigation into the hardness and microstructure relationship of an electrochemically deposited nc Ni–20 wt.% Fe alloy during high-pressure torsion was performed. In summary, the following conclusions are drawn:

(1) With increasing HPT shear strain, the Ni–20 wt. % Fe alloy experiences progressively strain hardening, softening and then hardening again.
(2) The hardness evolution of the material is primarily controlled by the evolution of the dislocation density. The two strain hardening stages are accompanied by an increase in the dislocation density while the softening stage is associated with a decrease in the dislocation density.
(3) The effect on the hardness of HPT-induced grain growth and detwinning is outweighed by the stronger role of the dislocations.

Acknowledgements

The authors are grateful for scientific and technical input and support from the Australian Microscopy & Microanalysis Research Facility node at the University of Sydney. This project is supported by the Australian Research Council [Grant No. DP0772880 (S.N., Y.B.W., and X.Z.L.)], the LDRD program of Los Alamos National Laboratory(H.Q.L.), the Office of Naval Research [Grant No. N00014-08-1-0405 (Y.H.Z. and E.J.L.)], the National Science Foundation of the United States (Grant No. DMR-0855009, T.G.L.) and the U.S. Army Research Office and Army Research Laboratory (Y.T.Z.). S.N. also appreciates support from the China Scholarship Council.

References

[1] R.Z. Valiev, I.V. Alexandrov, Y.T. Zhu, T.C. Lowe, J. Mater. Res. 17 (2002) 5–8.
[2] R.Z. Valiev, T.G. Langdon, Prog. Mater. Sci. 51 (2006) 881–981.
[3] A.P. Zhilyaev, T.G. Langdon, Prog. Mater. Sci. 53 (2008) 893–979.
[4] A.P. Zhilyaev, B.K. Kim, G.V. Nurislamova, M.D. Baró, J.A. Szpunar, T.G. Langdon, Scripta Mater. 46 (2002) 575–580.
[5] A.P. Zhilyaev, B.K. Kim, J.A. Szpunar, M.D. Baró, T.G. Langdon, Mater. Sci. Eng. A 391 (2005) 377–389.
[6] P.P.V. Liddicoat, X.Z. Liao, Y.H. Zhao, Y.T. Zhu, M.Y. Murashkin, E.J. Lavernia, R.Z. Valiev, S.P. Ringer, Nat. Commun. 1 (2010) 63.
[7] R.Z. Valiev, R.K. Islamgaliev, I.V. Alexandrov, Prog. Mater. Sci. 45 (2000) 103–189.
[8] X.Z. Liao, J.Y. Huang, Y.T. Zhu, F. Zhou, E.J. Lavernia, Philos. Magn. 83 (2003) 3065–3075.
[9] F. Torre. Dalla, R. Lapovok, J. Sandlin, P.F. Thomson, C.H.J. Davies, E.V. Pereloma, Acta Mater. 52 (2004) 4819–4832.
[10] Z. Horita, T. Fujinami, M. Nemoto, T.G. Langdon, Metall. Mater. Trans. A 31 (2000) 691–701.
[11] Y.T. Zhu, T.G. Langdon, JOM 56 (10) (2004) 58–63.
[12] C.Y. Yu, P.L. Sun, P.W. Kao, C.P. Cheng, Scripta Mater. 52 (2005) 359–363.
[13] Y.H. Zhao, J.F. Bingert, Y.T. Zhu, X.Z. Liao, R.Z. Valiev, Z. Horita, T.G. Langdon, Y.Z. Zhou, E.J. Lavernia, Appl. Phys. Lett. 92 (2008) 081903.
[14] B. Yang, H. Vehoff, A. Hohenwarter, M. Hafok, R. Pippan, Scripta Mater. 58 (2008) 790–793.
[15] D. Jia, K.T. Ramesh, E. Ma, Acta Mater. 51 (2003) 3495–3509.
[16] H.G.F. Wilsdorf, D. Kuhlmann-Wilsdorf, Mater. Sci. Eng. A 164 (1993) 1–14.
[17] S. Hariprasad, S.M.L. Sastry, K.L. Jerina, Acta Mater. 44 (1996) 383–389.
[18] F.A. Mohamed, Acta Mater. 51 (2003) 4107–4119.
[19] Y.B. Wang, X.Z. Liao, Y.H. Zhao, E.J. Lavernia, S.P. Ringer, Z. Horita, T.G. Langdon, Y.T. Zhu, Mater. Sci. Eng. A 527 (2010) 4959–4966.
[20] X.Z. Liao, A.R. Kilmametov, R.Z. Valiev, H.S. Gao, X.D. Li, A.K. Mukherjee, J.F. Bingert, Y.T. Zhu, Appl. Phys. Lett. 88 (2006) 021909.
[21] L. Li, T. Ungár, Y.D. Wang, G.J. Fan, Y.L. Yang, N. Jia, Y. Ren, G. Tichy, J. Lendvai, H. Choo, P.K. Liaw, Scripta Mater. 60 (2009) 317–320.
[22] G.J. Fan, L.F. Fu, H. Choo, P.K. Liaw, N.D. Browning, Acta Mater. 54 (2006) 4781–4792.
[23] A.P. Zhilyaev, A.A. Gimazov, E.P. Soshnikova, V. Révész, T.G. Langdon, Mater. Sci. Eng. A 489 (2008) 207–212.
[24] G.J. Fan, Y.D. Wang, L.F. Fu, H. Choo, P.K. Liaw, Y. Ren, N.D. Browning, Appl. Phys. Lett. 88 (2006) 171914.
[25] M. Legros, D.S. Gianola, K.J. Hemker, Acta Mater. 56 (2008) 3380–3393.
[26] Z.W. Shan, E.A. Stach, J.M.K. Wiezorek, J.A. Knapp, D.M. Follstaedt, S.X. Mao, Science 305 (2004) 654–657.
[27] Y.B. Wang, B.Q. Li, M.L. Sui, S.X. Mao, Appl. Phys. Lett. 92 (2008) 011903.
[28] H.M. Wen, Y.H. Zhao, Y. Li, O. Ertorer, R.Z. Valiev, E.J. Lavernia, Philos. Mag. 90 (2010) 4541–4550.
[29] Y.B. Wang, J.C. Ho, X.Z. Liao, H.Q. Li, S.P. Ringer, Y.T. Zhu, Appl. Phys. Lett. 94 (2009) 011908.
[30] Y.B. Wang, J.C. Ho, Y. Cao, X.Z. Liao, H.Q. Li, Y.H. Zhao, E.J. Lavernia, S.P. Ringer, Y.T. Zhu, Appl. Phys. Lett. 94 (2009) 091–911.
[31] L. Li, T. Ungár, Y.D. Wang, J.R. Morris, G. Tichy, J. Lendvai, Y.L. Yang, Y. Ren, H. Choo, P.K. Liaw, Acta Mater. 57 (2009) 4988–5000.
[32] S. Ni, Y.B. Wang, X.Z. Liao, S.N. Alhajeri, H.Q. Li, Y.H. Zhao, E.J. Lavernia, S.P. Ringer, T.G. Langdon, Y.T. Zhu, Scripta Mater. 64 (2011) 327–330.
[33] S. Cheng, Y.H. Zhao, Y.M. Wang, Y. Li, X.L. Wang, P.K. Liaw, E.J. Lavernia, Phys. Rev. Lett. 104 (2010) 255501.
[34] Y. Ivanisenko, L. Kurmanaeva, J. Weissmueller, K. Yang, J. Markmann, H. Rösner, T. Scherer, H.J. Fecht, Acta Mater. 57 (2009) 3391–3401.
[35] S. Cheng, Y.H. Zhao, Y.Z. Guo, Y. Li, Q.M. Wei, X.L. Wang, Y. Ren, P.K. Liaw, H. Choo, E.J. Lavernia, Adv. Mater. 21 (2009) 5001–5004.
[36] H.Q. Li, F. Ebrahimi, Mater. Sci. Eng. A 347 (2003) 93–101.
[37] N.E. Dowling, Mechanical Behavior of Materials, Pearson Education, New Jersey, 2007.
[38] F. Wetscher, R. Pippan, S. Strum, F. Kauffmann, C. Scheu, G. Dehm, Metall. Mater. Trans. A 37 (2006) 1963–1968.
[39] A.P. Zhilyaev, T.R. McNelley, T.G. Langdon, J. Mater. Sci. 42 (2007) 1517–1528.

[40] A.P. Zhilyaev, K. Oh-Ishi, T.G. Langdon, T.R. McNelley, Mater. Sci. Eng. A 410–411 (2005) 277–280.
[41] Y. Cao, Y.B. Wang, S.N. Alhajeri, X.Z. Liao, W.L. Zheng, S.P. Ringer, T.G. Langdon, Y.T. Zhu, J. Mater. Sci. 45 (2010) 765–770.
[42] Y. Cao, M. Kawasaki, Y.B. Wang, S.N. Alhajeri, X.Z. Liao, W.L. Zheng, S.P. Ringer, Y.T. Zhu, T.G. Langdon, J. Mater. Sci. 45 (2010) 4545–4553.
[43] Y.F. Shen, L. Lu, Q.H. Lu, Z.H. Jin, K. Lu, Scripta Mater. 52 (2005) 989–994.
[44] L. Lu, R. Shwaiger, Z.W. Shan, M. Dao, K. Lu, S. Suresh, Acta Mater. 53 (2005) 2169–2179.
[45] Y.B. Wang, M.L. Sui, E. Ma, Philos. Magn. Lett. 87 (2007) 935–942.
[46] J.P. Hirth, R.W. Balluffi, Acta Metall. 21 (1973) 929–942.
[47] X.Z. Liao, Y.H. Zhao, S.G. Srinivasan, Y.T. Zhu, R.Z. Valiev, D.V. Gunderov, Appl. Phys. Lett. 84 (2004) 592.
[48] V. Yamakov, D. Wolf, S.R. Phillpot, H. Gleiter, Acta Mater. 50 (2002) 5005–5020.
[49] Y.T. Zhu, X.Z. Liao, R.Z. Valiev, Appl. Phys. Lett. 86 (2005) 103112.
[50] Y.T. Zhu, J. Narayan, J.P. Hirth, S. Mahajan, X.L. Wu, X.Z. Liao, Acta Mater. 57 (2009) 3763–3770.
[51] J. Wang, N. Li, O. Anderoglu, X. Zhang, A. Misra, J.Y. Huang, J.P. Hirth, Acta Mater. 58 (2010) 2262–2270.
[52] V. Yamakov, D. Wolf, S.R. Phillpot, H. Gleiter, Acta Mater. 51 (2003) 4135–4147.
[53] X.L. Wu, Y.T. Zhu, Y.G. Wei, Q. Wei, Phys. Rev. Lett. 103 (2009) 205–504.
[54] V.B. Shenoy, R.V. Kukta, R. Phillips, Phys. Rev. Lett. 84 (2000) 1491–1494.
[55] R. Madec, B. Devincre, L.P. Kubin, Phys. Rev. Lett. 89 (2002) 255508.
[56] S. Billard, J.P. Fondère, B. Bacroix, G.F. Dirras, Acta Mater. 54 (2006) 411–421.
[57] X.X. Huang, N. Hansen, N. Tsuji, Science 312 (2006) 249–251.
[58] Z.W. Shan, R.K. Mishra, S.A.S. Asif, O.L. Warren, A.M. Minor, Nat. Mater. 7 (2008) 115–119.